Pramana – J. Phys. (2019) 93:31
https://doi.org/10.1007/s12043-019-1792-5

Performance of resistance in the variation on a nano thin film flow influenced by thermal deposition: The Buongiorno model

E N MARAJ*, Z IQBAL and JAMILA BIBI

Department of Mathematics, HITEC University, Taxila 47700, Pakistan
*Corresponding author. E-mail: ehnber@gmail.com; ehnber.naheed@hitecuni.edu.pk

MS received 25 September 2018; revised 1 February 2019; accepted 4 February 2019;
published online 30 May 2019

Abstract. In the current study, the flow of Casson liquid thin film, together with heat transfer towards a stretching surface extracting out from a narrow slit in the presence of a magnetic field, viscous dissipation and thermal radiation effects, is examined. The contribution of nanoparticles is investigated by employing the Buongiorno model. Mathematical modelling is carried out in the Cartesian coordinate system and similarity analysis is opted for simplification. The numerical analysis is performed in the reduced system using the shooting method. The effects of the prominent parameters are discussed using line and bar graphs. The key finding is that the temperature drop is prominent in the case of Casson nanofluid compared to the nanofluid.

Keywords. Variant thermophysical characteristics; viscous dissipation; Casson fluid; thin film flow.

PACS Nos 44.25.+f; 47.10.ad; 47.50.−d

1. Introduction

The flow of thin liquid coating and heat transfer are of immense significance because of their wide applications in industry, manufacturing and engineering procedures. Wire and fibre coating, polymer, chemical and food processes, designing of the several heat exchangers are some well-known examples where thin liquid film flow plays a significant role. Crane [1] originally studied the boundary layer flow towards a stretching horizontal surface. He pointed out the significant contribution of the stretching surface velocity on fluid flow and boundary layer thickness. After him, many researchers attempted to analyse several types of fluid flows along with heat transfer over linearly as well as nonlinearly stretching sheets in the presence of different physical phenomena such as magentohydrodynamics (MHD), porous medium, permeable stretching surface, mixed convection, thermal radiation, viscous dissipation, etc. Some of the remarkable contributions to literature in this regard are cited in refs [2–6]. The pioneer study of the MHD boundary layer flow within a thin liquid coating was carried out by Wang [7]. In his study, an asymptotic solution to the thin film flow was derived. He concluded that the non-dimensional unsteady parameter influences the boundary layer thickness and other fluid dynamic characteristics. After this initial work, many researchers [8–14] have explored the heat transfer of Newtonian as well as non-Newtonian liquid coating flow. Recently, El-Aziz and Afify [15] examined the impact of erratic thermal conductivity and viscosity on viscoelastic fluid transport within the liquid thin coating in the presence of an aligned magnetic field. Some recent work related to this are cited in refs [16–20].

The Casson fluid model proposed by Casson and Mill [21] is one of the non-Newtonian fluid models exhibiting the rheological characteristics of viscoplastic fluids such as colloidal suspensions, polymeric solutions, syrup, etc. It is worth mentioning here that for large values of Casson parameter γ, this model exhibits the behaviour of Newtonian fluid.

Keeping the aforementioned literature survey, the present paper focusses on examining the influence of variant thermophysical characteristics on nanofluid transport and heat transfer along with nanoparticles Brownian motion and thermophoresis phenomenon. Numerical procedure, specifically, shooting algorithm is used to compute velocity, temperature and concentration distributions. The impact of several emerging parameters on nanofluid flow, temperature and concentration is examined and discussed using graphs.

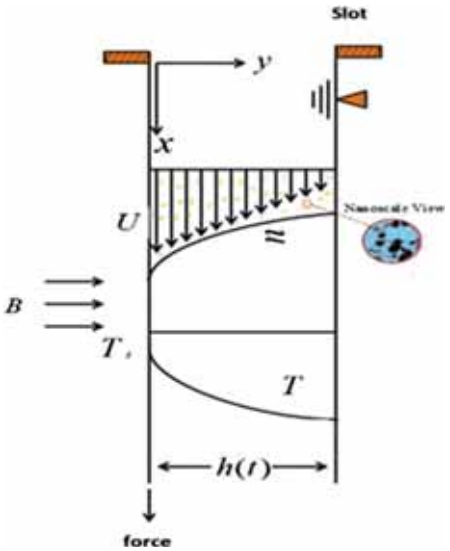

Figure 1. Geometry of the flow problem.

2. Problem formulation

Here the boundary layer flow of a Casson nanofluid within a thin liquid film towards the vertical stretching sheet emerging from a narrow slit placed at the origin is examined. Heat transfer along with fluid flow is considered in the presence of a variant external magnetic field $\bar{B}(x,t)$ applied normal to the flow direction. It is assumed that the magnetic Reynolds number of the flow is very small so that the induced magnetic field and Hall current effects are negligible. A Cartesian coordinate system is opted for the mathematical formulation. The x-axis is chosen in the direction of motion along the stretching surface and the y-axis is taken to be normal to the surface as shown in figure 1.

Accordingly, the fluid velocity in the component form is defined as

$$\bar{V} = [u(x,y), v(x,y), 0] \tag{1}$$

and the external applied magnetic field in the component form is defined as

$$\bar{B}(x,t) = [0, B(x,t), 0], \tag{2}$$

where u and v are the velocity components along the x and y directions, respectively and is introduced as [22]

$$B(x,t) = \frac{B_0}{\sqrt{1-\alpha t}}, \tag{3}$$

where B_0 is the constant uniform magnetic field and α (s^{-1}) is a material constant. To study the effects of variable viscosity, the Reynolds model [23] is taken into account, i.e.

$$\mu(T) = \mu_f e^{-\beta(T-T_0)}. \tag{4}$$

Here, μ_f is the Casson fluid viscosity and β (K^{-1}) (>0) is the material constant. The stretching velocity and surface temperature are taken to be of the following form:

$$U_s(x,t) = \frac{bx}{1-\alpha t},$$
$$T_s(x,t) = T_0 - T_{ref}\frac{bx^2}{2\nu}(1-\alpha t)^{-3/2}, \tag{5}$$

where b (s^{-1}) and α (s^{-1}) are constants, T_0 denotes slot temperature, T_{ref} stands for a reference temperature and $\nu = \mu_f/\rho$ is the kinematic viscosity. The extra stress tensor $\bar{S}$ for the Casson fluid model (according to Casson and Mill [21]) is defined as

$$\bar{S} = S_{ij} = \mu(T)\left(1 + \frac{1}{\gamma}\right)\bar{A}_1, \tag{6}$$

where γ is the Casson fluid parameter and $\bar{A}_1$ is the first Rivlin–Erickson tensor. It is worth mentioning here that when $\gamma \to \infty$, eq. (6) reduces to an extra stress tensor for the Newtonian fluid. The equations which govern the incompressible Casson nanofluid flow are defined in eqs (7)–(10):

$$\bar{\nabla}\cdot\bar{V} = 0, \tag{7}$$

$$\rho\left[\frac{\partial}{\partial t} + (\bar{V}\cdot\bar{\nabla})\right]\bar{V} = \text{div}\,\bar{\tau} + \bar{J}\times\bar{B} + g\beta(T-T_0) + g\beta(C-C_0), \tag{8}$$

$$\rho C_p\left[\frac{\partial T}{\partial t} + u\frac{\partial T}{\partial x} + v\frac{\partial T}{\partial y}\right] = \frac{\partial}{\partial y}\left(k(T)\frac{\partial T}{\partial y}\right) + \bar{\tau}\cdot\bar{L} - \frac{\partial Q_r}{\partial y} + \tau\left\{D_B\left(\frac{\partial C}{\partial y}\frac{\partial T}{\partial y}\right) + \frac{D_T}{T_0}\left(\frac{\partial T}{\partial y}\right)^2\right\}, \tag{9}$$

$$\frac{\partial C}{\partial t} + u\frac{\partial C}{\partial x} + v\frac{\partial C}{\partial y} = D_B\nabla^2 C + \frac{D_T}{T_0}\nabla^2 T, \tag{10}$$

in which eq. (7) is the conservation of mass, eq. (8) is the conservation of linear momentum in which (according to the Buongiorno model [24]) the last two terms on the right-hand side are the contribution of nanoparticles. Equations (9) and (10) are respectively the second law of thermodynamics and Fick's law of diffusion. Moreover, in the above expressions, g is the gravitational force, C is the nanoparticles concentration, C_0 is the ambient concentration, τ is the Cauchy stress tensor defined as $\tau = -p\bar{I} + \bar{S}$, $\bar{J}$ is the current density, $\bar{J}\times\bar{B}$ is the Lorentz force, T is the temperature, T_0 is the ambient temperature, C_p is the specific heat, D_B is the Brownian diffusion coefficient, D_T is the thermophoretic diffusion

coefficient and Q_r is the radiative heat flux after applying Rosseland approximation [25] which is defined as

$$Q_r = -\frac{4\sigma^*}{3k_1}\frac{\partial T^4}{\partial y}. \tag{11}$$

Under the assumption of reasonably small temperature differences within the thin liquid film, and applying Taylor series expansion to expand T^4 about T_0 and neglecting higher-order terms yields

$$T^4 \cong 4T_0^3 T - 3T_0^4 \tag{12}$$

and therefore

$$\frac{\partial Q_r}{\partial y} = -\frac{16\sigma^* T_0^3}{3k_1}\frac{\partial^2 T}{\partial y^2}, \tag{13}$$

where the Stefan–Boltzmann constant is denoted by σ^* and k_1 is the mean absorption coefficient. The effect of viscous dissipation after applying boundary layer approximation is expressed as

$$\bar{\tau}\cdot\bar{L} = \mu(T)\left(1+\frac{1}{\gamma}\right)\left(\frac{\partial u}{\partial y}\right)^2, \tag{14}$$

where $\bar{L} = \text{grad}(V)$ is the velocity gradient.

It is assumed that the thermophysical fluid properties are isotropic and constant except for the fluid viscosity and thermal conductivity which is taken to be temperature-dependent as follows [15]:

$$k(T) = k_0[1 + c(T - T_0)], \tag{15}$$

where k_0 is the constant thermal conductivity and c (K^{-1}) is the material constant. In the absence of a pressure gradient and after applying boundary layer approximation, eqs (7)–(10) can be expressed in component form as

$$\frac{\partial u}{\partial x} + \frac{\partial v}{\partial y} = 0, \tag{16}$$

$$\frac{\partial u}{\partial t} + u\frac{\partial u}{\partial x} + v\frac{\partial u}{\partial y} = \frac{1}{\rho}\frac{\partial}{\partial y}\left[\mu(T)\left(1+\frac{1}{\gamma}\right)\frac{\partial u}{\partial y}\right] - \frac{\sigma B^2}{\rho}u + g\beta(T - T_0) + g\beta(C - C_0), \tag{17}$$

$$\rho C_p\left[\frac{\partial T}{\partial t} + u\frac{\partial T}{\partial x} + v\frac{\partial T}{\partial y}\right] = \frac{\partial}{\partial y}\left(k_0[1 + c(T - T_0)]\frac{\partial T}{\partial y}\right) + \mu(T)\left(1+\frac{1}{\gamma}\right)\left(\frac{\partial u}{\partial y}\right)^2 + \frac{16\sigma^* T_0^3}{3k_1}\frac{\partial^2 T}{\partial y^2} + \tau\left\{D_B\left(\frac{\partial C}{\partial y}\frac{\partial T}{\partial y}\right) + \frac{D_T}{T_0}\left(\frac{\partial T}{\partial y}\right)^2\right\}, \tag{18}$$

$$u\frac{\partial C}{\partial x} + v\frac{\partial C}{\partial y} = D_B\frac{\partial^2 C}{\partial y^2} + \frac{D_T}{T_0}\frac{\partial^2 T}{\partial y^2}. \tag{19}$$

Here σ is the electric conductivity of the Casson fluid and the associated boundary conditions are expressed as

$$\begin{aligned} &u = U_s, \quad v = 0, \quad T = T_s, \\ &D_B\frac{\partial C}{\partial y} + \frac{D_T}{T_0}\frac{\partial T}{\partial y} = 0 \quad \text{at } y = 0, \\ &\frac{\partial u}{\partial y} = 0, \quad v = \frac{\partial h}{\partial t}, \quad \frac{\partial T}{\partial y} = 0, \quad \frac{\partial C}{\partial y} = 0 \quad \text{at } y = h. \end{aligned} \tag{20}$$

To reduce the nonlinear coupled system of partial differential equations (16)–(19), the following similarity variables are introduced:

$$\begin{aligned} &\eta = \sqrt{\frac{b}{\nu(1-\alpha t)}}y, \quad \psi(x,y,t) = \sqrt{\frac{b\nu}{(1-\alpha t)}}xf(\eta), \\ &\theta(\eta) = \frac{T - T_0}{T_s - T_0}, \quad \varphi(\eta) = \frac{C - C_0}{C_s - C_0}, \end{aligned} \tag{21}$$

where T_s and C_s are the temperature and concentration at the surface,

$$T = T_0 - \frac{T_{\text{ref}} b x^2}{2\nu(1-\alpha t)^{3/2}}\theta(\eta). \tag{22}$$

It is worth mentioning that expression (22) is valid only for $\alpha t < 1$. The relationship between fluid velocity components and stream function is defined as

$$u = \frac{\partial \psi}{\partial y} \quad \text{and} \quad v = -\frac{\partial \psi}{\partial x}. \tag{23}$$

Using relations (21) and (23), eq. (16) is identically satisfied and eqs (17)–(19) can be simplified as

$$\left(1+\frac{1}{\gamma}\right)e^{-\lambda\theta}f''' - \left(1+\frac{1}{\gamma}\right)\lambda e^{-\lambda\theta}\theta' f'' - S\left(f' + \frac{\eta}{2}f''\right) - f'^2 + ff'' - Mf' + \text{Gr}\,\theta + \text{Br}\,\varphi = 0, \tag{24}$$

$$\left(\delta\theta + \frac{1}{N}\right)\theta'' + \delta\theta'^2 + \text{Pr}\,\text{Ec}\left(1+\frac{1}{\gamma}\right)e^{-\lambda\theta}f''^2 - \text{Pr}\left[\frac{S}{2}(3\theta + \eta\theta') + 2\theta f' - f\theta'\right] + \text{Nb}\,\varphi'\theta' + \text{Nt}\,\theta'^2 = 0, \tag{25}$$

$$\varphi'' + \text{Sc}\,f\varphi' + \frac{\text{Nt}}{\text{Nb}}\theta'' = 0. \tag{26}$$

Here, prime indicates the differentiation with respect to η. Moreover, the non-dimensional parameters λ, S, M, Gr, Br, δ, Pr, Ec, R, Nb, Nt and Sc are the variable viscosity, unsteadiness, magnetic parameters, local

temperature and local nanoparticle Grashof numbers, variable thermal conductivity parameter, Prandtl number, Eckert number, thermal radiation parameter, Brownian motion parameter, thermophoretic diffusion parameter and Schmidt number and are defined as

$$\lambda = \beta(T_s - T_0), \quad S = \frac{\alpha}{b}, \quad M = \frac{\sigma B_0^2}{b\rho},$$

$$\mathrm{Gr} = \frac{g\beta(T_s - T_0)(1-\alpha t)^2}{b^2 x},$$

$$\mathrm{Br} = \frac{g\beta(C_s - C_0)(1-\alpha t)^2}{b^2 x}, \quad \delta = c(T_s - T_0),$$

$$\mathrm{Pr} = \frac{\rho C_p \nu}{k_0}, \quad \mathrm{Ec} = -\frac{2\nu b}{C_p T_{\mathrm{ref}}(1\ -\alpha t)^{1/2}},$$

$$R = \frac{k_0 k_1}{4\sigma^* T_0^3}, \quad \mathrm{Nb} = \frac{\tau D_B (C_s - C_0)}{k_0},$$

$$\mathrm{Nt} = \frac{\tau D_T (T_s - T_0)}{k_0 T_0}, \quad N = \frac{3R}{3R+4}, \quad \mathrm{Sc} = \frac{\nu}{D_B}. \tag{27}$$

It is worth mentioning here that when $R \to \infty$, $N = 1$. Consequently, eq. (25) does not take into account the effect of thermal radiation. Moreover, when $M = \delta = \mathrm{Ec} = 0$, $N = 1$ and $\gamma \to \infty$ [4], the problem is retained as a special case. Boundary conditions defined in eq. (20) are simplified to

$$f'(0) = 1, \quad f(0) = 0, \quad \theta(0) = 1,$$

$$\varphi'(0\ ) + \frac{\mathrm{Nt}}{\mathrm{Nb}}\theta'(0) = 0, \quad f''(\beta) = 0, \quad \theta'(\beta) = 0,$$

$$\varphi'(\beta) = 0, \quad f(\beta) = \frac{\beta S}{2}. \tag{28}$$

The similarity variable η on the free surface is taken to be β. Thus, from eq. (21),

$$\beta = \left(\frac{b}{\nu(1\ -\alpha t)}\right)^{1/2} h. \tag{29}$$

The meaningful physical quantities such as local skin friction coefficient C_f, local Nusselt number Nu_x and Sherwood number Sh_x are defined as

$$C_f = \frac{\tau_w}{\rho(U_s)^2}, \ \mathrm{Nu}_x = \frac{x q_w}{k_0(T_w - T_0\ )},$$

$$\mathrm{Sh}_x = \frac{x q_m}{D_B(C_s - C_0)}, \tag{30}$$

where τ_w, q_w and q_m represent surface shear stress, heat and mass fluxes defined in the following expressions:

$$\tau_w = -\left(\mu_B + \frac{p_y}{\sqrt{2\pi_c}}\right)\left(\frac{\partial u}{\partial y}\right)\Big|_{y=0},$$

$$q_w = -\left(\left(k + \frac{16\,\sigma^* T_0^3}{3k_1}\right)\frac{\partial T}{\partial y}\right)\Big|_{y=0},$$

$$q_m = -D_B \frac{\partial C}{\partial y}\Big|_{y=0}. \tag{31}$$

The physical quantities defined in eq. (30), in terms of similarity variables, are expressed as

$$\sqrt{\mathrm{Re}_x} C_f = -\left(\frac{1\ +\gamma}{\gamma}\right) f''(0),$$

$$\frac{\mathrm{Nu}_x}{\sqrt{\mathrm{Re}_x}} = -\left(\delta + \frac{1}{N}\right)\theta'(0),$$

$$\mathrm{Re}_x^{-1/2}\mathrm{Sh}_x = -\varphi'(0), \tag{32}$$

where $\mathrm{Re}_x = x U_s/\nu$ is the local Reynolds number.

3. Solution methodology

The simplified system of nonlinear coupled eqs (24)–(26) subject to the boundary conditions (28) is numerically solved by means of shooting technique together with the Runge–Kutta fourth-order procedure. Firstly, the higher-order differential equations are downgraded to a system of first-order differential equations by incorporating the following substitutions:

$$\begin{pmatrix} f \\ f' \\ f'' \\ f''' \\ \theta \\ \theta' \\ \theta'' \\ \varphi \\ \varphi' \\ \varphi'' \end{pmatrix} = \begin{pmatrix} y_1 \\ y_2 = y_1' \\ y_3 = y_2' \\ y_3' \\ y_4 \\ y_5 = y_4' \\ y_5' \\ y_6 \\ y_7 = y_6' \\ y_7' \end{pmatrix}, \tag{33}$$

so that we obtain the following system of first-order differential equations:

$$\begin{pmatrix} y_1' \\ y_2' \\ y_3' \\ y_4' \\ y_5' \\ y_6' \\ y_7' \end{pmatrix} = \begin{pmatrix} y_2 \\ y_3 \\ \dfrac{\mathrm{e}^{\lambda y_4}}{(1+(1/\gamma))}\left(\begin{array}{c}\lambda \mathrm{e}^{-\lambda y_4}\left(1+\dfrac{1}{\gamma}\right)y_5 y_3 + S\left(y_2+\dfrac{\eta}{2}y_3\right)+y_2^2-y_1 y_3 \\ +My_2-\mathrm{Gr}y_4-\mathrm{Br}y_6\end{array}\right) \\ y_5 \\ \dfrac{1}{(\delta y_4+(1/N))}\left(\begin{array}{c}-\delta y_5^2-\mathrm{Pr\,Ec}\left(1+\dfrac{1}{\gamma}\right)\mathrm{e}^{-\lambda y_4}y_3^2-\mathrm{Nb}y_7 y_5-\mathrm{Nt}y_5^2 \\ +\mathrm{Pr}\left(\dfrac{S}{2}(3y_4+\eta y_5)+2y_2 y_4-y_1 y_5\right)\end{array}\right) \\ y_7 \\ -\mathrm{Sc}y_1 y_7-\dfrac{\mathrm{Nt}}{\mathrm{Nb}}y_5' \end{pmatrix}, \tag{34}$$

and the reduced problem is transformed into an initial value problem by incorporating additional initial conditions in terms of shooting parameters, i.e.

$$\begin{pmatrix} y_1(0) \\ y_2(0) \\ y_3(0) \\ y_4(0) \\ y_5(0) \\ y_7(0) \\ y_7(0) \end{pmatrix} = \begin{pmatrix} 0 \\ 1 \\ s_1 \\ 1 \\ s_2 \\ -\dfrac{\mathrm{Nt}}{\mathrm{Nb}}y_5(0) \\ s_3 \end{pmatrix}, \tag{35}$$

where s_1, s_2 and s_3 are the shooting parameters. Computational analysis is performed using the mathematics software MAPLE and iterative results are obtained for an accuracy of 10^{-4}.

4. Graphical results and discussion

In this section, the effect of the emerging non-dimensional parameters of significance such as the unsteadiness parameter (S), Hartmann number (M), variable viscosity parameter (λ), local-temperature Grashof number (Gr), local nanoparticle Grashof number (Br), variable thermal conductivity parameter (δ), thermal radiation parameter (N), Brownian motion parameter (Nb), thermophoretic parameter (Nt) and the Prandtl (Pr) and Eckert (Ec) numbers, respectively, on Casson nanofluid velocity, temperature and concentration distributions are examined and displayed through graphs. Here the graphs are plotted for two types of fluid models, namely, Casson nanofluid and nanofluid. In these graphs, the solid lines represent the results for Casson nanofluid while the dashed lines represent the results of the nanofluid. It is worth mentioning here that when the Casson nanofluid parameter γ approaches a very large number, mathematically, when $\gamma \to \infty$, the Casson nanofluid model exhibits the results for the nanofluid.

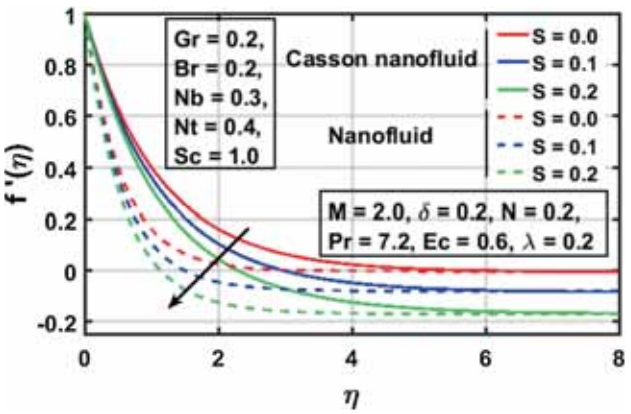

Figure 2. Effect of unsteadiness parameter S on $f'(\eta)$.

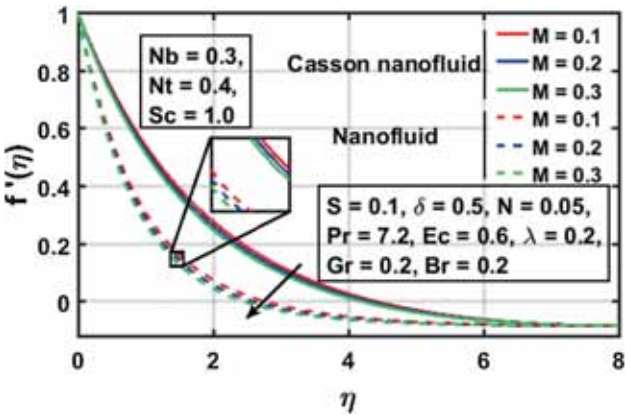

Figure 3. Influence of M on velocity.

Figures 2–6 are drawn for fluid velocity for distinct values of unsteadiness parameter, Hartmann number, variable viscosity parameter, Gr and Br, respectively. Figure 2 is plotted to explore the effect of unsteadiness parameter on the fluid flow and it is seen that an increase in S contributes to decelerated fluid flow. This decrease in velocity is significantly more in the nanofluid than in the Casson nanofluid. This trend is noted because

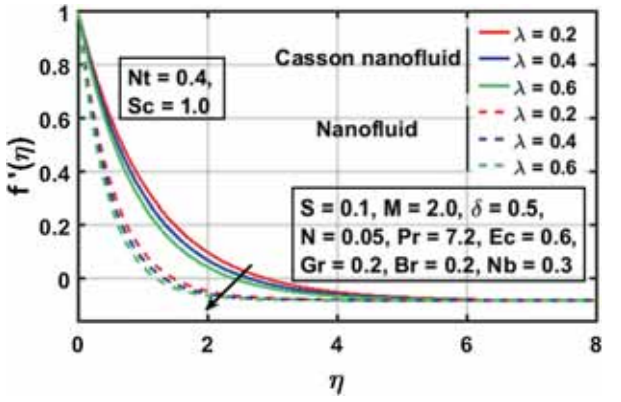

Figure 4. Impact of λ on $f'(\eta)$.

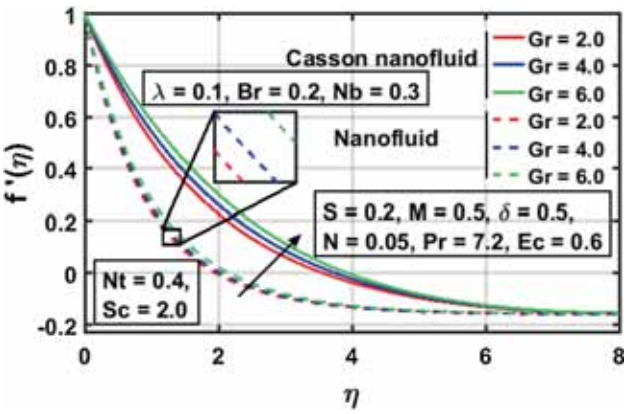

Figure 5. Effect of Gr on the fluid flow.

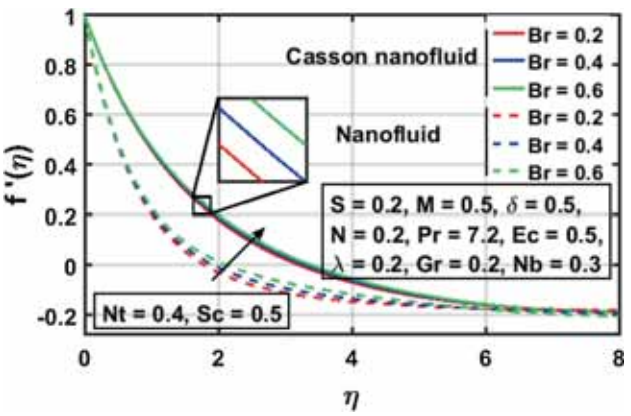

Figure 6. Influence of Br on velocity.

of the fact that the rising value of the unsteadiness parameter indicates a decrease in film thickness. The influence of an external magnetic field is explored in figure 3. It is depicted that the presence of a magnetic field resists fluid flow and, consequently, fluid velocity decreases. This decrease is dominant in the case of the nanofluid. Figure 4 is plotted for the distinct values of the temperature-dependent viscosity parameter.

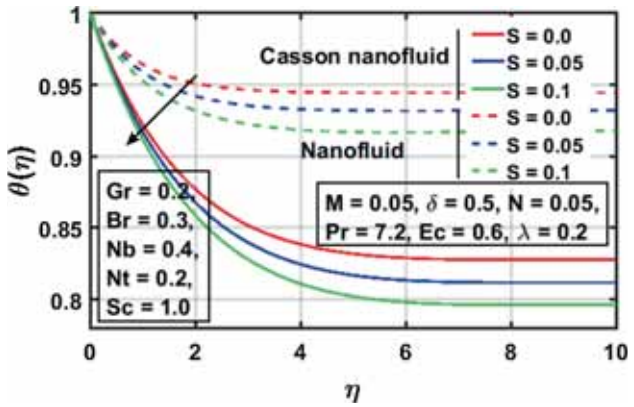

Figure 7. Temperature distributions for various values of S.

From this figure, it is concluded that an increase in λ indicates an increase in variable viscosity which contributes to the rise in resistance to the fluid flow and, subsequently, fluid velocity lessens. This decrease in velocity is significantly more in the nanofluid than in the Casson nanofluid. The impact of local-temperature Grashof number Gr is depicted in figure 5. It is revealed that an increase in Gr contributes to the accelerating fluid flow and this increase in velocity is prominently more in the Casson nanofluid. The reason behind this trend is that Gr is the ratio of buoyancy to viscous forces, and thus an increase in it indicates less viscous forces acting on the fluid and, consequently, fluid flow accelerates. Figure 6 is drawn for the rising values of local nanoparticles Grashof number Br for the velocity profile. From this figure, it is depicted that increasing values of Br lead to an increase in fluid velocity. This trend is seen because, an increase in Br indicates an increase in motile nanoparticle concentration which contributes to accelerated fluid flow. This increase in velocity is significantly more in the nanofluid than in the Casson nanofluid.

Figures 7–15 are drawn to examine the effect of prominent parameters such as the unsteadiness parameter, thermal radiation parameter N, Prandtl number, Eckert number, variable thermal conductivity parameter δ, variable viscosity parameter λ, Brownian motion parameter Nb and thermophoretic parameter Nt, respectively, on the temperature profile. Figure 7 is plotted for the rising values of unsteadiness parameter and a drop in temperature is witnessed. Moreover, this temperature drop is prominent when the Casson nanofluid is taken into account. This happens due to the fact that small values of the Casson fluid parameter indicate an increase in the plastic dynamic viscosity which resists the fluid flow and, subsequently, the temperature increases. The influence of an applied external magnetic field on temperature is explored in figure 8. It is observed that an increase in Hartmann number results in an increase in

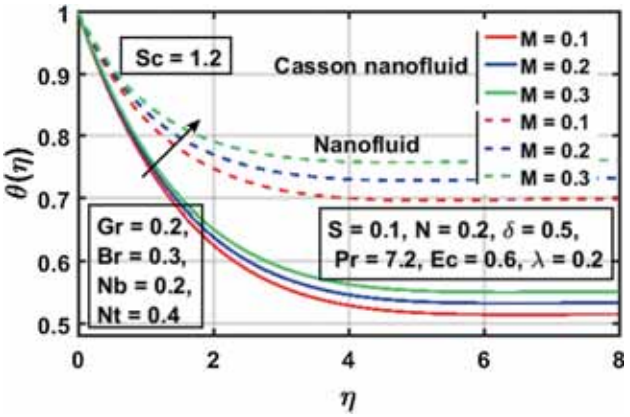

Figure 8. Effect of M on $\theta(\eta)$.

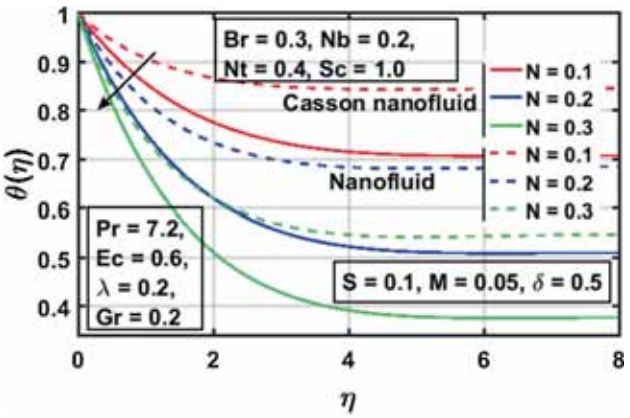

Figure 9. Influence of N on temperature.

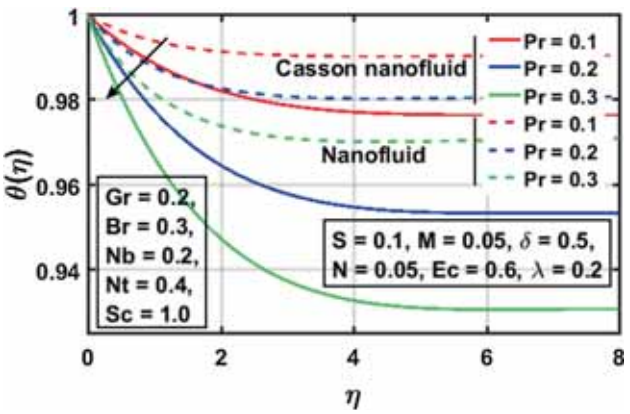

Figure 10. Temperature distributions for various values of Pr.

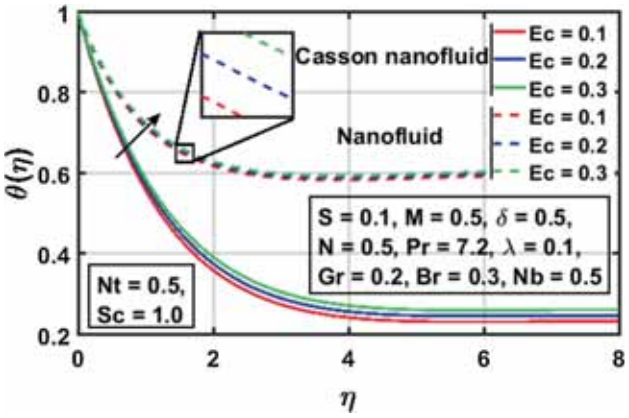

Figure 11. Effect of Ec on $\theta(\eta)$.

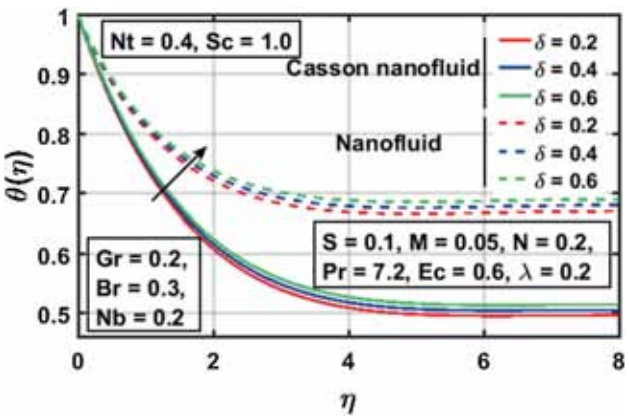

Figure 12. Temperature distributions for increasing values of δ.

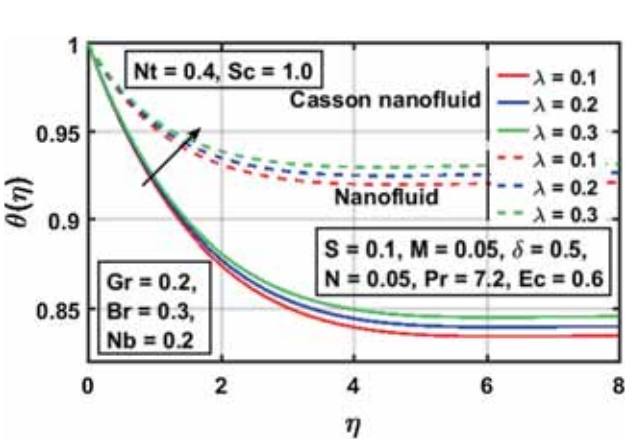

Figure 13. Temperature distributions for increasing values of λ.

fluid temperature. The main reason is that the magnetic field contributes to the increasing frictional drag which leads to an upsurge in fluid temperature. From this figure, it is depicted that the increase in temperature is significantly high in the nanofluid compared to the Casson nanofluid. The effect of thermal radiation parameter N on the temperature field is illustrated in figure 9. It is observed that an increase in N contributes to a drop in temperature distribution. This trend is reported because an increase in N improves the efficacy of conduction within the thin liquid film. Moreover, this temperature drop is prominent in Casson nanofluid compared to the nanofluid. Figure 10 is drawn to study the effect

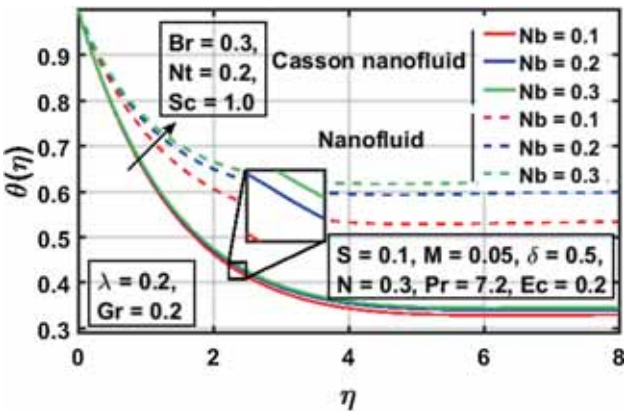

Figure 14. Temperature distributions for various values of Nb.

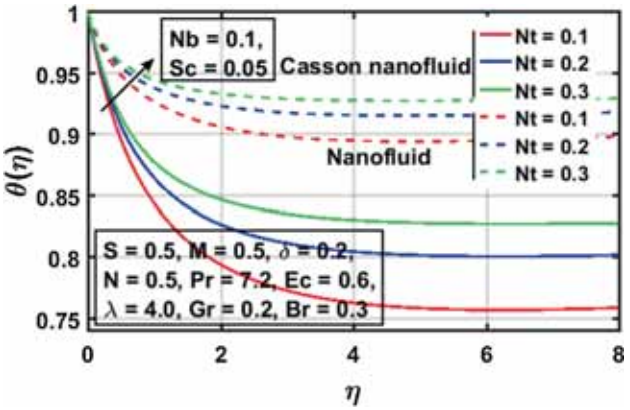

Figure 15. Temperature distributions for distinct values of Nt.

of Prandtl number on temperature and a reduction in temperature distribution is reported for the rising values of Pr. This happens because Pr is the ratio of momentum to thermal diffusivity. Thus, an increase in Pr indicates a low thermal diffusivity and, subsequently, the temperature drops. Moreover, this drop in temperature is reasonably more in the case of the Casson nanofluid. The influence of viscous dissipation on the temperature profile is studied through the Eckert number whose effect on temperature is shown in figure 11. It is depicted that the temperature increases with an increase in Ec. This happens because, Ec represents the effect of heat dissipation due to the viscous force and an increase in Eckert number indicates an increase in viscous dissipation which leads to an upsurge in fluid temperature. Furthermore, from this figure, it is concluded that the increase in temperature is dominant in a nanofluid compared to the Casson nanofluid. Figure 12 is plotted to explore the influence of temperature-dependent thermal conductivity on temperature distribution. From this figure, it is concluded that temperature rises with an increase in variable thermal conductivity parameter δ. This happens

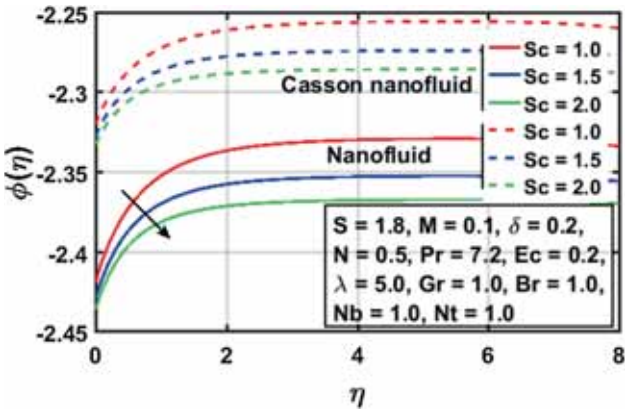

Figure 16. Concentration distributions for increasing values of Sc.

because the thermal conductivity is taken to be directly proportional to the temperature difference and hence an increase in temperature leads to an increase in thermal conductivity and, consequently, the fluid temperature rises. Moreover, it is also revealed that this increase in temperature is prominently more in the nanofluid than in the Casson nanofluid. The influence of the variable viscosity parameter on temperature distribution is studied in figure 13. It is revealed that the fluid temperature rises with an increase in λ, the reason behind this trend is that an increase in λ indicates a rise in variable viscosity which offers more resistance to fluid flow and, as a result, the fluid temperature upsurges. Moreover, this increase in temperature is significantly dominant in the nanofluid. Figure 14 is drawn to examine the effect of Brownian motion of nanoparticles on temperature distribution. It is depicted that an increase in Nb leads to a rise in the temperature profile. This happens due to the fact that the rising values of Nb indicate an increase in the random motion of nanoparticles, and hence, to an increase in particle collisions and, as a result, the fluid temperature increases. This temperature boost is dominant in the nanofluid compared to the Casson nanofluid. The thermophoresis effect of nanoparticles on fluid temperature is plotted in figure 15, for distinct values of Nt. This figure reveals that the temperature increases with an increase in thermophoretic parameter within the thin liquid film. This rise in temperature is dominant in the nanofluid.

Figures 16–18 are plotted to explore the effect of Schmidt number Sc, Brownian motion parameter Nb and thermophoretic parameter Nt, respectively, on the nanoparticles concentration profile. Figure 16 is plotted for the rising values of Sc for ϕ. From this figure, it is concluded that the concentration of nanoparticles drops with an increase in Sc. This happens mainly because Sc is the ratio of momentum to mass diffusivity. Thus, an increase in Sc indicates an

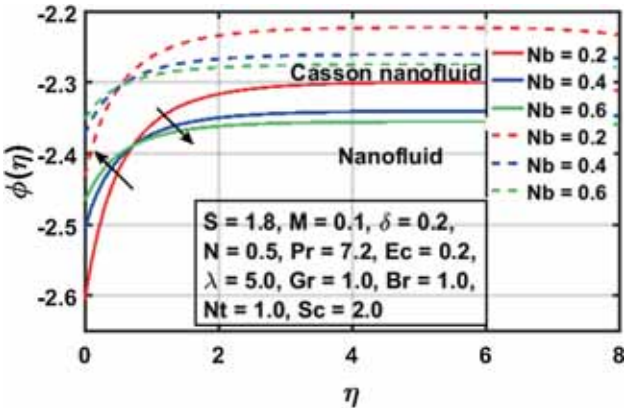

Figure 17. Concentration distributions for increasing values of Nb.

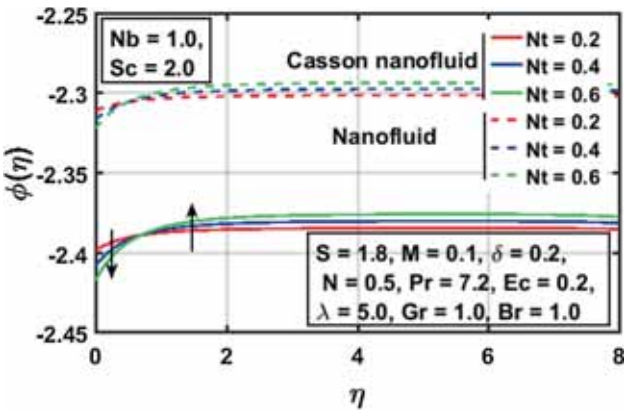

Figure 18. Concentration distributions for various values of Nt.

increase in momentum diffusivity and, consequently, the concentration of nanoparticles drops. The effect of nanoparticles on Brownian motion is examined in figure 17. It is depicted that near the opening of the slit, the concentration of nanoparticles increases with an increase in Nb and afterwards, a contrasting trend is witnessed. Figure 18 is plotted to examine the effect of thermophoresis parameter Nt on the nanoparticles concentration profile. This figure reveals a contrasting trend as compared to figure 17, i.e. the concentration drops near the opening of the slip and afterwards, it increases.

Figures 19–25 are the bar charts for the skin friction coefficient, and the Nusselt and Sherwood numbers for distinct values of emerging significant parameters. From the bar charts displayed in figures 19 and 20, it is concluded that the Grashof number Br of the local nanoparticles and the Casson nanofluid parameter contribute to the reduced shear stress at the surface while the shear stress increases for the rising values of the local-temperature Grashof number Gr, unsteadiness parameter, variable viscosity parameter and Hartmann number, respectively. Figures 21–24 are the bar graphs

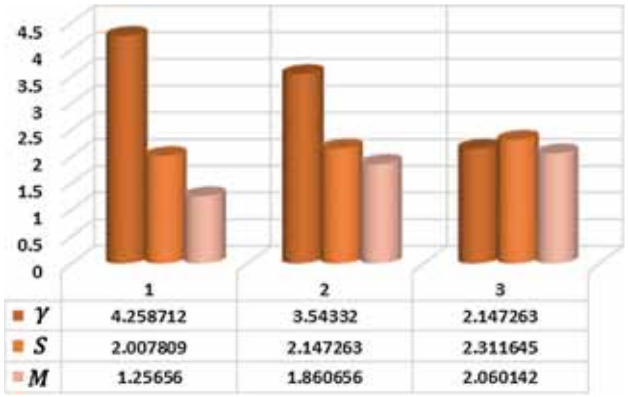

Figure 19. Effect of γ, S and M on skin friction coefficient.

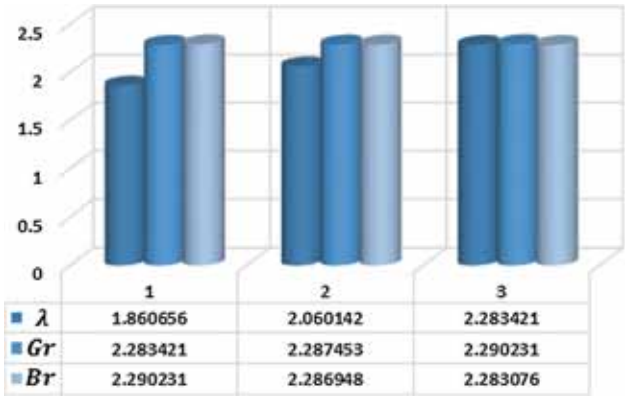

Figure 20. Effect of λ, Gr and Br on skin friction coefficient.

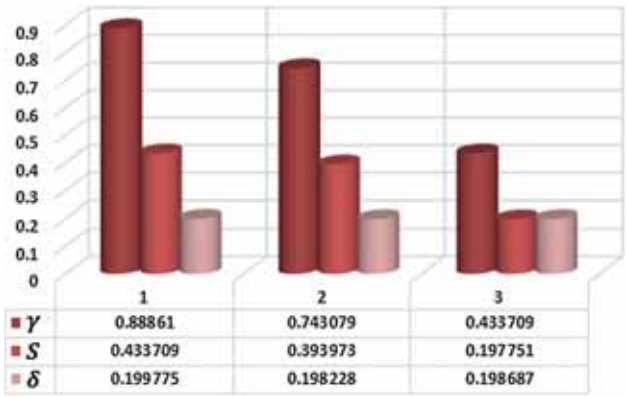

Figure 21. Effect of γ, S and δ on Nusselt number.

drawn for the Nusselt number against the rising values of pertinent parameters. From these bar graphs, it is evident that the variable thermal conductivity, Prandtl number, nanoparticles Brownian motion and the local nanoparticles Grashof numbers played a role in increasing the surface heat flux rate, whereas it decreases for the rising values of variable viscosity, Casson nanofluid, unsteadiness parameters, Eckert and local nanoparticles

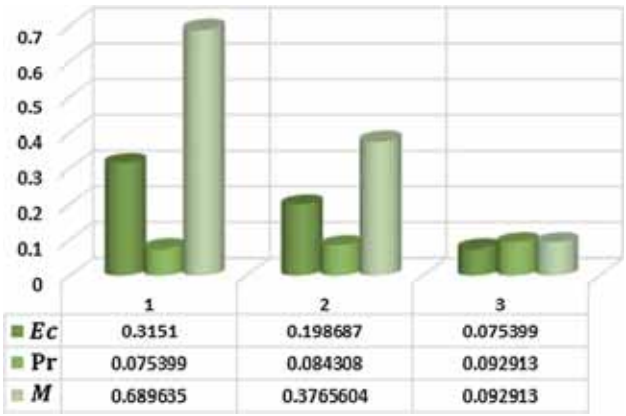

Figure 22. Effect of Ec, Pr and M on Nusselt number.

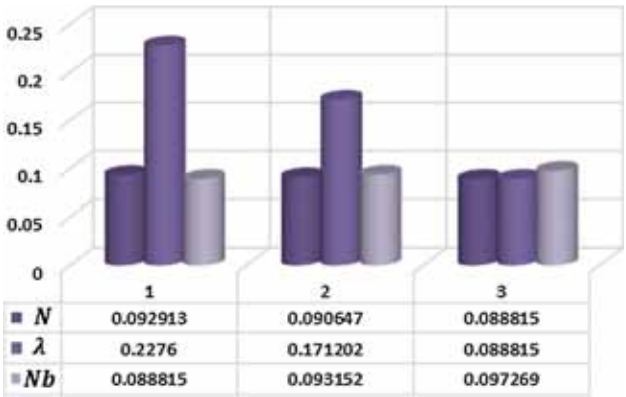

Figure 23. Effect of N, λ and Nb on Nusselt number.

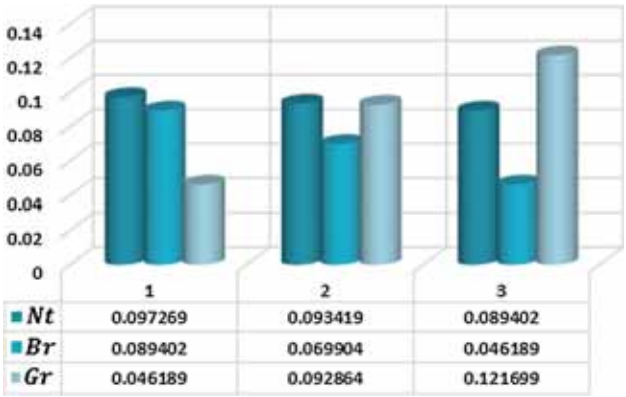

Figure 24. Effect of Nt, Br and Gr on Nusselt number.

Grashof numbers, magnetic field, nanoparticles thermophoresis and thermal radiation, respectively. The effects of important parameters on the Sherwood number are studied using the bar chart displayed in figure 25. It is revealed that the Sherwood number increases with an increase in the Schmidt number and the thermophoretic parameter while a contrasting behaviour is reported for the rising values of the Casson nanofluid and nanoparticle Brownian motion parameters.

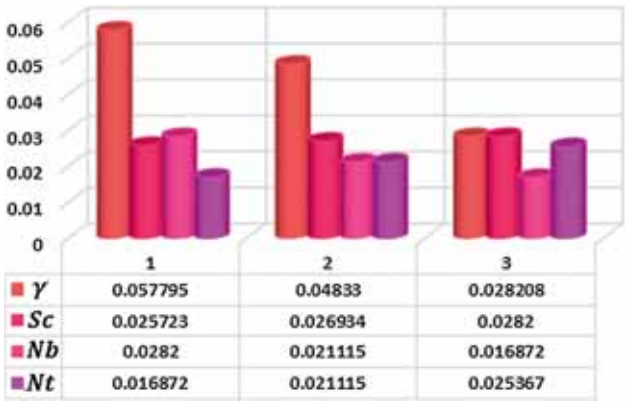

Figure 25. Variation in Sherwood number.

5. Concluding remarks

In this paper, the impact of temperature-dependent viscosity and thermal conductivity effect on heat transfer and MHD Casson nanofluid flow within a thin liquid film towards an unsteady extending surface in the presence of thermal radiation were examined. The key findings include:

- Fluid flow decelerated with an increase in S as well as the magnetic field and variable viscosity parameter. It is worth mentioning here that when the Casson nanofluid parameter γ approaches a very large number, mathematically, when $\gamma \to \infty$, the Casson nanofluid model exhibits the results for the nanofluid. Furthermore, the decrease in fluid velocity was significantly more in the nanofluid than in the Casson nanofluid.
- Local temperature and local nanoparticle Grashof numbers contributed to the accelerated fluid flow and this increase in velocity was prominently more in the Casson nanofluid.
- Rising values of the unsteadiness parameter led to a drop in temperature. Moreover, this temperature drop was slightly more when the Casson nanofluid was taken into account.
- An increase in the Hartmann number resulted in an increase in fluid temperature. Furthermore, the increase in temperature was significantly higher in the nanofluid than in the Casson nanofluid.
- Temperature rose with an increase in variable thermal conductivity δ and viscosity λ parameters.
- An increase in N contributed to a drop in temperature distribution. Moreover, this temperature drop is prominent in the Casson nanofluid compared to the nanofluid.
- Temperature distribution decreased for the rising values of Pr.

- Temperature increased with an increase in Ec. Furthermore, the increase in temperature was dominant in the nanofluid compared to the Casson fluid.
- Nanoparticle Brownian motion parameter Nb and the thermophoretic parameter Nt contributed to the upsurge in temperature distribution.
- Near the slit opening, the concentration of nanoparticles increased with an increase in the Brownian motion parameter Nb.
- A contrasting trend was reported for the rising values of Nt.
- The local nanoparticles Grashof number Br and the Casson nanofluid parameter contributed to the reduced shear stress at the surface while it increased for the rising values of the local-temperature Grashof number Gr, unsteadiness parameter, variable viscosity parameter and Hartmann number, respectively.
- The variable thermal conductivity, Prandtl number, nanoparticle Brownian motion and local-temperature Grashof number played a role in increasinging the surface heat flux rate, whereas it decreases for rising values of variable viscosity, Casson nanofluid, unsteadiness parameters, Eckert and local nanoparticles Grashof numbers, magnetic field, nanoparticles thermophoresis and thermal radiation.
- The magnitude of the Sherwood number rose with an increase in the Schmidt number and the thermophoretic parameter while contrasting behaviour was reported for the rising values of the Casson nanofluid and the nanoparticle Brownian motion parameters.

References

[1] L J Crane, *J. Appl. Math. Phys.* **21**, 645 (1970)
[2] S Iram, M Nawaz and A Ali, *Pramana – J. Phys.* **91**: 47 (2018)
[3] H I Andersson, J B Aareth, N Braud and B S Dandapat, *J. Non-Newton. Fluid Mech.* **62**, 1 (1996)
[4] H I Andersson, J B Aarseth and B S Dandapat, *Int. J. Heat Mass Transf.* **43**, 69 (2000)
[5] B S Dandapat, B Santra and H I Andersson, *Int. J. Heat Mass Transf.* **46**, 3009 (2003)
[6] C H Chen, *Heat Mass Transf.* **39**, 791 (2003)
[7] C Wang, *Heat Mass Transf.* **42**, 759 (2006)
[8] I C Liu and H I Andersson, *Int. J. Therm. Sci.* **47**, 766 (2008)
[9] M S Abel, N Mahesha and J Tawade, *Appl. Math. Model.* **33**, 3430 (2009)
[10] M S Abel, J Tawade and M M Nandeppanavar, *Int. J. Non-Linear Mech.* **44**, 990 (2009)
[11] H Xu, I Pop and X C You, *Int. J. Heat Mass Transf.* **60**, 646 (2013)
[12] B S Dandapat, A Kitamura and B Santra, *Z. Angew Math. Phys.* **57**, 623 (2006)
[13] B S Dandapat, S Maity and A Kitamura, *Int. J. Non-Linear Mech.* **43**, 880 (2008)
[14] S Maity, *Int. J. Heat Mass Transf.* **70**, 819 (2014)
[15] M A El-Aziz and A A Afify, *Braz. J. Phys.* **46**, 516 (2016)
[16] Z Iqbal, E Azhar and E N Maraj, *Chaos Solitons Fractals* **114**, 312 (2018)
[17] Z Iqbal, E Azhar, E N Maraj and Z Mehmood, *Commun. Theor. Phys.* **70**, 239 (2018)
[18] E N Maraj, S Shaiq and Z Iqbal, *J. Mol. Liq.* **262**, 275 (2018)
[19] E N Maraj, Z Iqbal and S Shaiq, *Int. J. Hydro. Energy,* **43**, 10915 (2018)
[20] K U Rehman, N U Saba, M Y Malik and I Zehra, *Eur. Phys. J. E* **41**, 37 (2018)
[21] N A Casson and C C Mill (eds) *Rheology of disperse systems* (Pergamon Press, New York, 1959) p. 84
[22] M A El-Aziz, *Meccanica* **45**, 97 (2010)
[23] B S Dandapat, B Santra and K Vajravelu, *Int. J. Heat Mass Transf.* **50**, 991 (2007)
[24] J Buongiorno, *ASME J. Heat Transf.* **128**, 240 (2006)
[25] M Q Brewster, *Thermal radiative transfer properties* (Wiley, London, 1972)